frontiers in Chemistry

ORIGINAL RESEARCH
published: 09 October 2018
doi: 10.3389/fchem.2018.00473

Development of n-Type Porphyrin Acceptors for Panchromatic Light-Harvesting Fullerene-Free Organic Solar Cells

Un-Hak Lee[1†], Wisnu Tantyo Hadmojo[2†], Junho Kim[2], Seung Hun Eom[1], Sung Cheol Yoon[1], Sung-Yeon Jang[2*] and In Hwan Jung[2*]*

[1] Division of Advanced Materials, Korea Research Institute of Chemical Technology, Daejeon, South Korea, [2] Department of Chemistry, Kookmin University, Seoul, South Korea

OPEN ACCESS

Edited by:
Chuanlang Zhan, Institute of Chemistry (CAS), China

Reviewed by:
Francesca Di Maria, Istituto di Nanotecnologia (NANOTEC), Italy
Yongsheng Liu, Nankai University, China

****Correspondence:***
Sung Cheol Yoon
yoonsch@krict.re.kr
Sung-Yeon Jang
syjang@kookmin.ac.kr
In Hwan Jung
ihjung@kookmin.ac.kr

[†] These authors have contributed equally to this work

Specialty section:
This article was submitted to Organic Chemistry, a section of the journal Frontiers in Chemistry

Received: *16 June 2018*
Accepted: *18 September 2018*
Published: *09 October 2018*

Citation:
Lee U-H, Hadmojo WT, Kim J, Eom SH, Yoon SC, Jang S-Y and Jung IH (2018) Development of n-Type Porphyrin Acceptors for Panchromatic Light-Harvesting Fullerene-Free Organic Solar Cells. Front. Chem. 6:473. doi: 10.3389/fchem.2018.00473

The development of n-type porphyrin acceptors is challenging in organic solar cells. In this work, we synthesized a novel n-type porphyrin acceptor, P_{Zn}-TNI, via the introduction of the electron withdrawing naphthalene imide (NI) moiety at the meso position of zinc porphyrin (P_{Zn}). P_{Zn}-TNI has excellent thermal stability and unique bimodal absorption with a strong Soret band (300–600 nm) and weak Q-band (600–800 nm). The weak long-wavelength absorption of P_{Zn}-TNI was completely covered by combining the low bandgap polymer donor, PTB7-Th, which realized the well-balanced panchromatic photon-to-current conversion in the range of 300–800 nm. Notably, the one-step reaction of the NI moiety from a commercially available source leads to the cheap and simple n-type porphyrin synthesis. The substitution of four NIs in P_{Zn} ring induced sufficient n-type characteristics with proper HOMO and LUMO energy levels for efficient charge transport with PTB7-Th. Fullerene-free organic solar cells based-on PTB7-Th:P_{Zn}-TNI were investigated and showed a promising PCE of 5.07% without any additive treatment. To the best of our knowledge, this is the highest PCE in the porphyrin-based acceptors without utilization of the perylene diimide accepting unit.

Keywords: porphyrin acceptors, n-type porphyrins, organic solar cells, non-fullerene acceptors, panchromatic absorption

INTRODUCTION

For decades, organic solar cells (OSCs) have been studied as a portable and low-cost power generator due to their unique advantages: light-weight, use of earth-abundant organic materials, solution-processability and flexibility. The power conversion efficiency (PCE) of OSCs, an important parameter to determine the performance of the OSCs, has been continuously improved by optimization of light-harvesting in active layers and hole/electron charge transport pathways (Zhan et al., 2015; Zhao J. et al., 2016; Lin et al., 2017; Che et al., 2018; Hou et al., 2018). In the 2000s, low-bandgap polymer donors and n-type fullerene acceptors blended OSCs were developed to make broad absorption in the active layer. Polymer donors showing a strong absorption coefficient were responsible for light-harvesting and exciton generation, while the n-type fullerenes effectively separate and transfer the electrons to the electrode (Kim et al., 2006; Liang et al., 2010; Li et al., 2012; Liao et al., 2013). However, this was not enough to cover all the visible band by blending polymer

donors and fullerene acceptors. In the 2010s, new types of OSCs replaced the fullerenes with strong light-harvesting organic non-fullerene acceptors (NFAs). The active layer was composed of organic donors and NFAs, called fullerene-free OSCs (Cheng et al., 2017; Lin et al., 2017; Tang et al., 2018; Yan et al., 2018). Due to the strong absorption of both NFAs and organic donors in the visible area, their complementary absorption is important to achieve panchromatic photon-to-current conversion in the active layer. There are several successful strategies for panchromatic absorption in the visible and near infra-red area. The most common approach is mixing wide-bandgap donors and low-bandgap small-molecule NFAs such as ITIC (Zhao W. et al., 2016, 2017; Lin et al., 2017; Yao et al., 2017; Zhao F. et al., 2017). Another approach is mixing low-bandgap donors and wide-bandgap NFAs (e.g., blending of PTB7-Th and perylene-diimide (PDI)-based acceptor) (Wu et al., 2016; Duan et al., 2017; Liang et al., 2017; Eom et al., 2018). The red-dye PDIs enable a strong absorption in the short-wavelength area of 400–600 nm, while showing effective n-type characteristics.

As a new approach for panchromatic absorption in an active layer, utilization of a nature-inspired porphyrin dye has recently emerged in OSCs.(Gao et al., 2015; Li et al., 2016; Hadmojo et al., 2018) The porphyrin dyes have peculiar bimodal absorption characteristics composed of Soret and Q bands; strong transition from ground state (S0) to second excited state (S2) yields the Soret band, while the weak transition from S0 to first excited state (S1) provides the Q-band. Thus, the strong Soret absorption of porphyrin dyes enables efficient short-wavelength absorption in the 400–600 nm, which can be blended with low-bandgap donors having a dominant absorption in the 600–800 nm for panchromatic absorption. In addition, the long-wavelength absorption of the Q-band intensifies the light harvesting in the low bandgap area where abundant solar flux exists. However, most of the developed artificial porphyrin derivatives are p-type materials and only a few porphyrin derivatives currently show n-type characteristics with a promising PCEs over 5% (Hadmojo et al., 2017; Zhang et al., 2017). Exploring new structures for n-type porphyrin materials is challenging in fullerene-free OSCs.

In this study, we synthesized a novel porphyrin acceptor, P_{Zn}-TNI, via Sonogashira coupling of 5,10,15,20-tetrakis-ethynyl porphyrin Zinc (II) (P_{Zn}) and 4-bromo-N-(2-ethylhexyl)-1,8-naphthalimide (NI). NI is easily synthesized from the commercially available 4-bromo-1,8-naphthalic anhydride. This one-step reaction is beneficial in terms of time and cost for synthesizing the star-shape molecules that require an excess of NIs. Since the NI has n-type characteristics, the substitution of NIs to the four meso positions of P_{Zn} enables the excellent n-type properties as an electron acceptor. The ethyne π-bridge unit is incorporated between NI and P_{Zn} to increase the backbone planarity. The synthesized P_{Zn}-TNI showed excellent thermal stability with 5% weight loss temperature of 412°C and showed unique bimodal absorption behavior with maximum peaks at 479 nm and 719 nm. The uncovered UV-Vis absorption spectrum from P_{Zn}-TNI is completely covered by the blending of a polymer donor, PTB7-Th, which resulted in the panchromatic photon-to-current conversion from 300 to 800 nm in OSCs. The planar backbone structure of P_{Zn}-TNI assists the sizable face-on orientation in the PTB7-Th:P_{Zn}-TNI blend film without additive treatment, which resulted in the highest PCE of 5.07% (V_{OC} = 0.72 V, J_{SC} = 13.84 mA cm^{-2}, and fill factor = 0.51) in the additive-free OSCs. The excessive ordering of PTB7-Th:P_{Zn}-TNI film via pyridine additive rather reduced the photovoltaic performances. Our successful utilization of NI moiety in the P_{Zn} core will broaden and diversify the synthetic approaches for developing high-efficiency porphyrin acceptors.

EXPERIMENTAL

Synthesis

5,10,15,20-tetrakis-ethynyl porphyrin Zinc (II) (3): Macrocyclic porphyrin compound 1 was synthesized according to the reported general procedure (Yen et al., 2006). Compound 1 (0.90 g, 1.29 mmol) and zinc acetate (2.4 g, 13.1 mmol) were dissolved in the co-solvent (200 ml) of dichloromethane:methanol = 9:1 v/v%. The resulting mixture was refluxed at 65°C for 24 h. After removing the solvents, the remaining solid was rinsed with dichloromethane (300 mL) to give a purple solid compound 2 (0.65 g, yield: 62%). Without further purification, compound 2 was directly used to make compound 3. Compound 2 (0.60 g, 0.79 mmol) was dissolved in 100 mL anhydrous tetrahydrofuran (THF). Tetra-n-butylammonium fluoride solution 1.0 M in THF (3.6 ml, 3.6 mmol) was slowly added to the reaction mixture. The resulting mixture was stirred at room temperature for 4 h. After removing the solvents, the crude solid product was rinsed sequentially with methanol, dichloromethane, water and acetone. After drying the dark purple solid product 3 (180 mg, yield: 49%), it was immediately used in the next step to prevent the coupling reaction between the two terminal alkynes. ^{1}H NMR (THF-d_6, 400 MHz, ppm): δ 9.60 (s, 2H), 5.37 (s, 1H),

N,*N*'-(2-hexyldecyl) 4-bromo naphthalene imide (4): 2-Hexyldecyl amine (2.4 g, 9.93 mmol) was added to the suspension of 4-bromo-1,8-naphthalic anhydride (2.5 g, 9.03 mmol) in dry ethanol (50 mL). The reaction mixture was refluxed overnight at 110°C, and then cooled down to room temperature. After evaporating the solvents, the remaining crude solid was purified using column chromatography on silica gel with an eluent of CH_2Cl_2:n-hexane = 4:1 to give a yellow solid compound 4 (3.0 g, 66%). ^{1}H NMR ($CDCl_3$, 400 MHz, ppm): δ 8.65 (d, J = 6.4 Hz, 1H), 8.56 (d, J = 7.6 Hz, 1H), 8.40 (d, J = 8.0 Hz, 1H), 8.03 (d, J = 7.6 Hz, 1H), 7.82 (m, 1H), 4.14 (t, J = 8.0 Hz, 2H), 1.70 (m, 1H), 1.24 (br, 27H), 0.87 (t, J = 7.2 Hz, 3H).

P_{Zn}-TNI: Compound 3 (100 mg, 0.212 mmol), compound 4 (1.06 g, 2.12 mmol), $Pd_2(dba)_3$ (40 mg, 0.044 mmol) and $AsPh_3$ (100 mg, 0.33 mmol) were dissolved in dry THF (15 mL) and triethylamine (15 mL). The reaction mixture was stirred at 65°C for 4 days under N_2 atmosphere, and then quenched by distilled water. The organic layer was extracted using dichloromethane and water, and then the moisture in the organic solution was removed by Na_2SO_4. After evaporating the solvents, the solid residue was purified by column chromatography using an eluent of CH_2Cl_2:n-hexane = 4:1. Then it was further purified using recycling size exclusion chromatography to give a deep green solid P_{Zn}-TNI (290 mg, 75%). ^{1}H NMR (THF-d_6, 400 MHz,

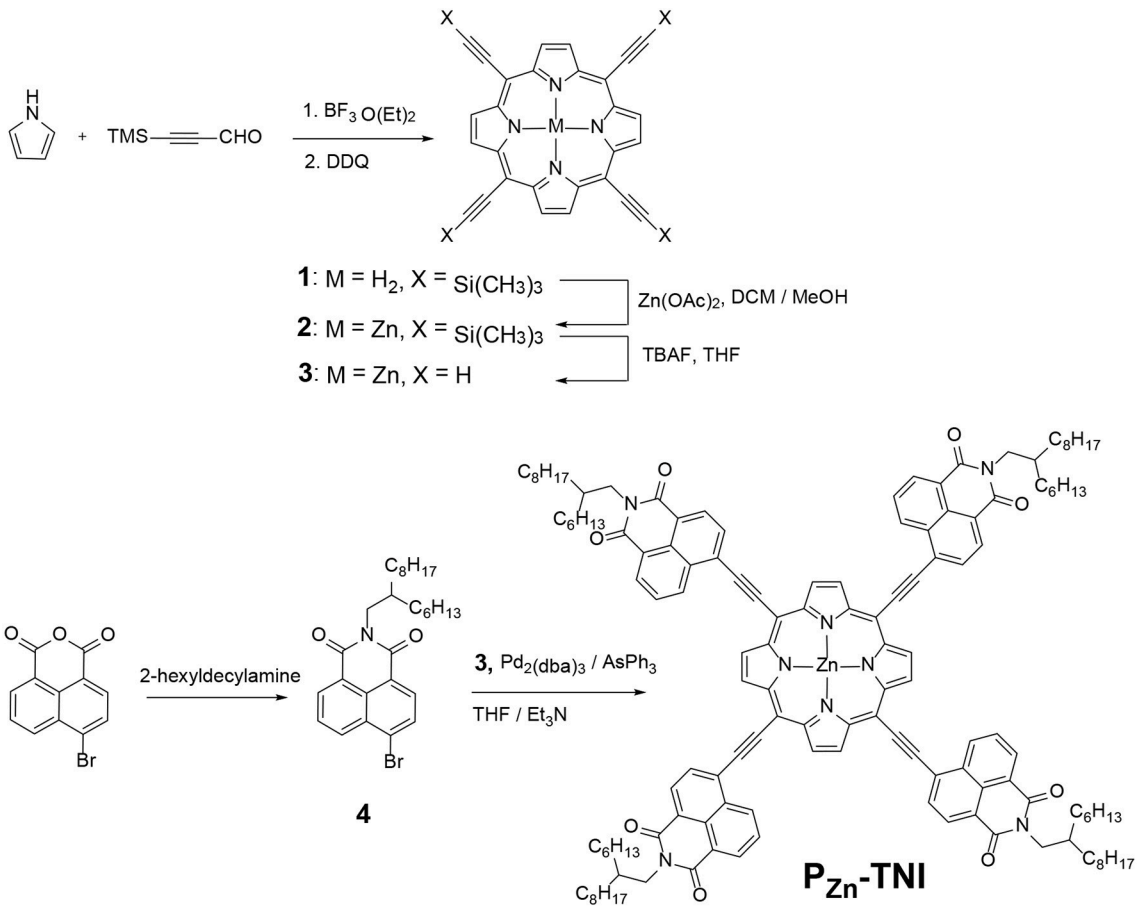

SCHEME 1 | Synthetic route for n-type porphyrin acceptor, P_{Zn}-TNI.

ppm): δ 9.02 (br, 2H), 8.85 (br, 1H), 8.40 (d, $J = 4.8$ Hz, 1H), 8.28 (d, $J = 5.6$ Hz, 1H), 8.19 (br, 1H), 7.88 (br, 1H), 4.24 (m, 2H), 1.92 (m, 1H), 1.39 (br, 27H), 0.96 (m, 3H). ^{13}C NMR (THF-d_6, 100 MHz, ppm): δ 163.58, 163.32, 149.75, 131.61, 131.49, 130.46, 130.18, 128.58, 128.35, 127.90, 124.02, 123.05, 102.08, 101.88, 96.30, 41.51, 33.14, 31.09, 31.05, 31.02, 30.99, 30.92, 30.87, 30.61, 29.22, 28.66, 23.82, 14.71. MALDI-TOF-MS: m/z: calcd. for $C_{140}H_{160}N_8O_8Zn$: 2145.17 $[M]^+$; found 2145.994.

RESULTS AND DISCUSSION

The synthetic procedure of P_{Zn}-TNI was recorded in **Scheme 1** and in the Supporting Information (SI) in detail. The porphyrin ring 1 was synthesized from pyrrole and 3-(trimethylsilyl)propiolaldehyde in the presence of $BF_3{\cdot}Et_2O$ followed by oxidation with 2,3-dichloro-5,6-dicyano-1,4-benzoquinone (DDQ). The zinc porphyrin (P_{Zn}) compound 2 was obtained using $Zn(OAc)_2$. The deprotection of TMS group by tetra-n-butylammonium fluoride (TBAF) was performed immediately before synthesizing the final acceptor, P_{Zn}-TNI. 4-Bromo-1,8-naphthalic anhydride purchased from Sigma-Aldrich was alkylated with 2-hexyldexylamine to give a compound 4. This one-step reaction to prepare the electron withdrawing NI unit is highly beneficial in terms of time and cost for achieving the n-type porphyrins. The final porphyrin acceptor, P_{Zn}-TNI, was achieved via Sonogashira coupling with P_{Zn} compound 3 and excess of NI compound 4, which was identified by ^{1}H-NMR and matrix assisted laser desorption/ionization time-of-flight mass spectrometry (MALDI-TOF-MS) (**Figures S1**–**S4**). The synthesized P_{Zn}-TNI showed excellent solubility in common organic solvents such as tetrahydrofuran (THF), dichloromethane (DCM), and chloroform (CF). In addition, it has excellent thermal stability, which was determined by thermal gravimetric analysis (TGA), with a 5% weight loss temperature (T_{5d}) of 412°C under an N_2 atmosphere (**Figure S5**).

Absorption spectra of P_{Zn}-TNI were measured in solution and the film state, as shown in **Figure 1**. P_{Zn}-TNI exhibited clear bimodal absorption composed of the Soret band (300 – 600 nm) and Q-bands (600–800 nm); the maximum absorption peaks of P_{Zn}-TNI were 479 and 713 nm in solution, and 478 and 719 nm in the film. The absorption of P_{Zn}-TNI was complementary to that of the low-bandgap donor polymer, PTB7-Th, which induced a well-balanced short- and long-wavelength absorption in the entire wavelength of 300–800 nm (**Figure 2B**). Notably, the film of P_{Zn}-TNI showed broadened

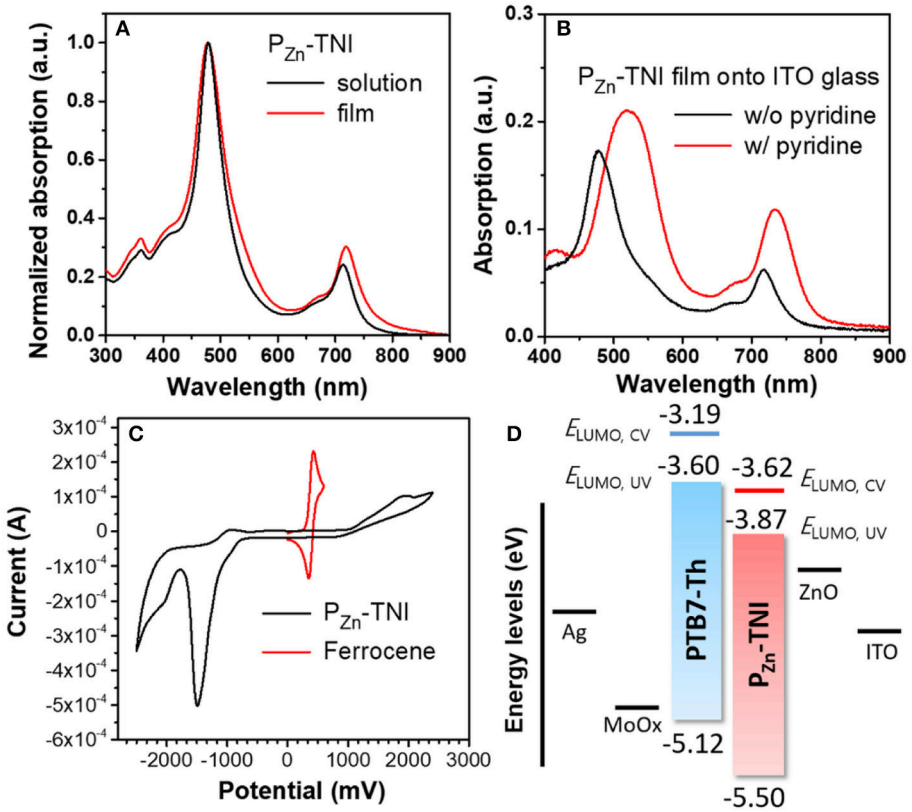

FIGURE 1 | Absorption spectra of PZn-TNI **(A)** in chloroform and in the film on the quartz plate, and **(B)** on ITO glass with or without pyridine additive. **(C)** Cyclic voltammogram of PZn-TNI, and **(D)** energy diagram of the PTB7-Th:PZn-TNI device.

and red-shifted Q-band absorption spectra compared to that in solution, indicating the enhanced intermolecular π-π stacking in the film state. Since the planar NIs and P_{Zn} are connected by an sp-hybridized ethyne π-bridge, P_{Zn}-TNI possesses a highly planar conjugated backbone for efficient intermolecular stacking. The optical bandgap (E_g^{opt}) of P_{Zn}-TNI was 1.63 eV, which was calculated from the absorption onset wavelength of 761 nm in the film. We previously reported the pyridine additive effect on the molecular ordering of porphyrin derivatives; pyridine enhances the intermolecular ordering of porphyrin derivatives via coordination to the zinc (Hadmojo et al., 2017). As shown in **Figure 1B**, the absorption of P_{Zn}-TNI was significantly broadened and red-shifted compared to that without pyridine treatment, resulting in the bathochromic shift of 42 nm in the Soret band and 15 nm in the Q-band. This supports our previous hypothesis for the pyridine effect on the molecular ordering and confirms that pyridine enhances the intermolecular ordering of P_{Zn}-TNI in the film states.

To evaluate the energy levels of P_{Zn}-TNI, the highest occupied molecular orbital (HOMO) energy levels and the lowest unoccupied molecular orbital (LUMO) energy levels were measured using cyclic voltammetry. The oxidation and reduction onset potentials of P_{Zn}-TNI were 1.07 and −0.80 V, respectively, which corresponds to HOMO levels ($E_{HOMO,CV}$) and LUMO levels ($E_{LUMO,CV}$) of −5.50 and −3.62 eV, respectively. The optical LUMO energy level ($E_{LUMO,UV}$) was calculated to be −3.87 eV from $E_{HOMO,CV}$ and E_g^{opt} of P_{Zn}-TNI. The energy diagram of the PTB7-Th and P_{Zn}-TNI was shown in **Figure 1D**, and the $E_{HOMO,CV}$, $E_{LUMO,CV}$, and $E_{LUMO,UV}$ of polymer donor (PTB7-Th) were taken from our previous measurement (Zhang et al., 2015; Hadmojo et al., 2016). The LUMO energy level of P_{Zn}-TNI is suitable for electron transport from PTB7-Th to P_{Zn}-TNI, while the HOMO of P_{Zn}-TNI is appropriate for hole transport from P_{Zn}-TNI to PTB7-Th (Marcus, 1963; Clarke and Durrant, 2010). The optical and electrochemical properties of P_{Zn}-TNI are summarized in **Table 1**.

Porphyrin acceptor-based fullerene-free OSCs were fabricated by blending PTB7-Th and P_{Zn}-TNI (**Figure 2A**). The current density-voltage (*J-V*) characteristic of PTB7-Th:P_{Zn}-TNI devices was investigated via changing the weight ratio between PTB7-Th and P_{Zn}-TNI, and the photovoltaic performance was optimized at the weight ratio of 1:1.5 w/w. The photovoltaic properties are summarized in **Figure 2C**, **Figure S6**, and **Table 2**. The best PCE of 5.07% was achieved with a V_{OC} of 0.72 V, a J_{SC} of 13.84 mA cm^{-2}, and FF of 0.51 (**Figure 2C**). As shown in **Figure 2D**, the external quantum efficiency (EQE) spectra of PTB7-Th:PZn-TNI devices cover the entire visible area of 300–800 nm and

TABLE 1 | Optical and electrochemical properties of P_{Zn}-TNI.

	UV-Vis absorption				Cyclic voltammetry				
	[a]Solution	[b]Film							
	λ_{max} (nm)	λ_{max} (nm)	λ_{onset} (nm)	[c]E_g^{opt} (eV)	E_{ox} (V)	E_{red} (V)	[d]$E_{HOMO, CV}$ (eV)	$E_{LUMO, CV}$ (eV)	[e]$E_{LUMO, UV}$ (eV)
P_{Zn}-TNI	479, 713	478, 719	761	1.63	1.07	−0.80	−5.50	−3.62	−3.87

[a]*Chloroform solution.*
[b]*Film on a quartz plate.*
[c]*Bandgap calculated from the film-state absorption onset wavelength (λ_{onset}).*
[d]*HOMO levels determined from E_{ox} of the first oxidation potential of P_{Zn}-TNI.*
[e]*LUMO levels calculated from $E_{HOMO, CV}$ and E_g^{opt}.*

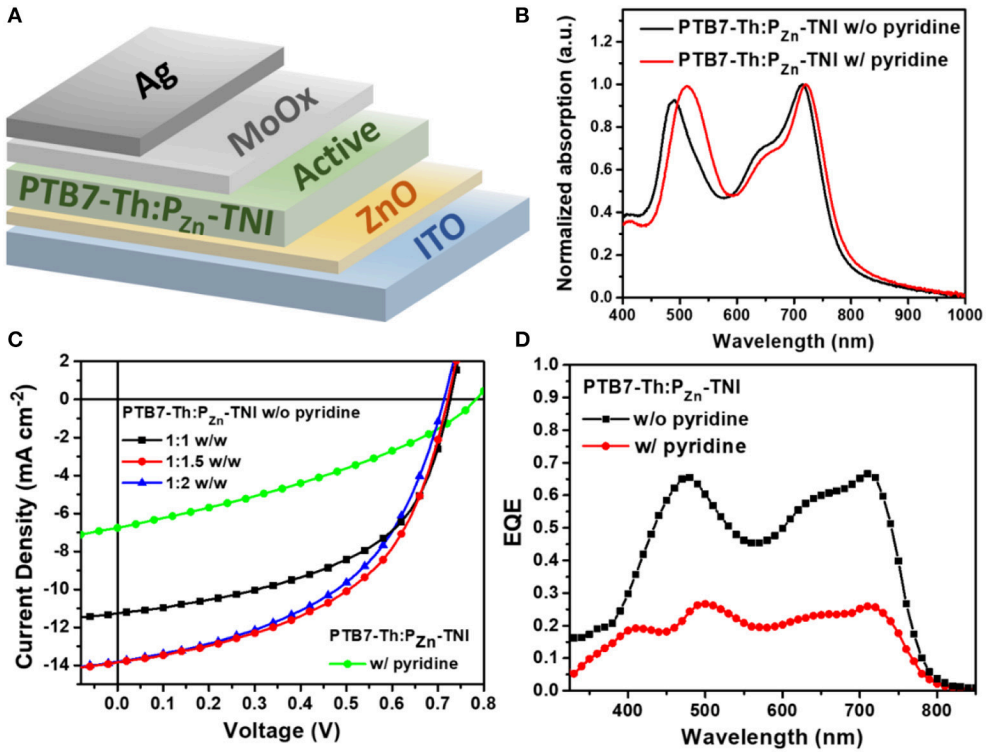

FIGURE 2 | (A) Device structure of PTB7-Th:P_{Zn}-TNI based OSCs, **(B)** absorption spectra of PTB7-Th:P_{Zn}-TNI active layer, **(C)** *J-V* characteristics of additive-free OSCs depending on the weight ratio between PTB7-Th and P_{Zn}-TNI, and the *J-V* curve of pyridine-treated OSCs at the weight ratio of PTB7-Th:PZn-TNI = 1:1.5 w/w. **(D)** the EQE spectra of PTB7-Th:P_{Zn}-TNI devices.

showed the panchromatic photon-to-current conversion due to the complementary solar flux absorption between PTB7-Th and PZn-TNI. Notably, the additive-free film-formation process provided superior photovoltaic performance compared to the pyridine-assisted one as shown in **Figure 2C**. As shown in **Figure 2D**, the EQE was increased in the entire wavelength, which indicates that hole/electron transport properties of both PTB7-Th and P_{Zn}-TNI are improved in the additive-free devices.

To understand the charge recombination mechanisms of PTB7-Th:P_{Zn}-TNI devices in the presence and absence of pyridine additive, the *J-V* characteristics were investigated as a function of the illumination intensity. The power law dependence of J_{SC} on the illumination intensity is generally expressed as $J_{SC} \propto I^{\alpha}$, where I is the light intensity and α is an exponential factor (**Figure 3A**) (Blom et al., 2007; Azmi et al., 2016). The α value of the PTB7-Th:P_{Zn}-TNI devices was close to unity regardless of additive treatment, indicating the negligible bimolecular recombination in PTB7-Th:P_{Zn}-TNI devices. However, the V_{OC} vs. illumination intensity was highly affected by the pyridine treatment. Assuming there is no trap-assisted recombination under an open-circuit condition, the slope of V_{OC} vs. the illumination intensity produces 1.00 kT/q (Mihailetchi et al., 2006). The higher value of kT/q indicates the more probability of trap-assisted recombination under an open-circuit condition (Mandoc et al., 2007; Azmi et al., 2016). As shown in **Figure 3B**,

TABLE 2 | Photovoltaic properties of PTB7-Th:P_{Zn}-TNI devices.

PTB7-Th:P_{Zn}-TNI		μ_h ($cm^2\ V^{-1}\cdot s^{-1}$)	μ_e ($cm^2\ V^{-1}\cdot s^{-1}$)	V_{OC} (V)	J_{SC} (mA cm^{-2})	FF	PCE (PCE_{ave})[a](%)
No additives	1:1	–	–	0.73	11.25	0.52	4.29 (3.97)
	1:1.5	2.9×10^{-4}	2.5×10^{-6}	0.72	13.84	0.51	5.07 (4.85)
	1:2	–	–	0.71	13.81	0.49	4.82 (4.59)
1% (v/v) pyridine	1:1.5	2.4×10^{-4}	1.3×10^{-6}	0.78	6.76	0.34	1.82 (1.61)

[a]*Average PCEs more than 10 devices.*

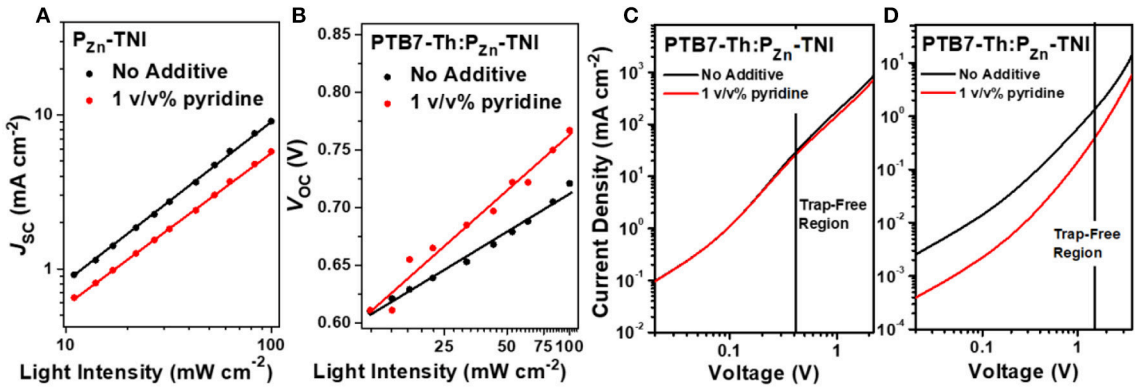

FIGURE 3 | (A) J_{SC} and **(B)** V_{OC} as a function of the illumination intensity. SCLC mobility of **(C)** hole-only and **(D)** electron-only devices.

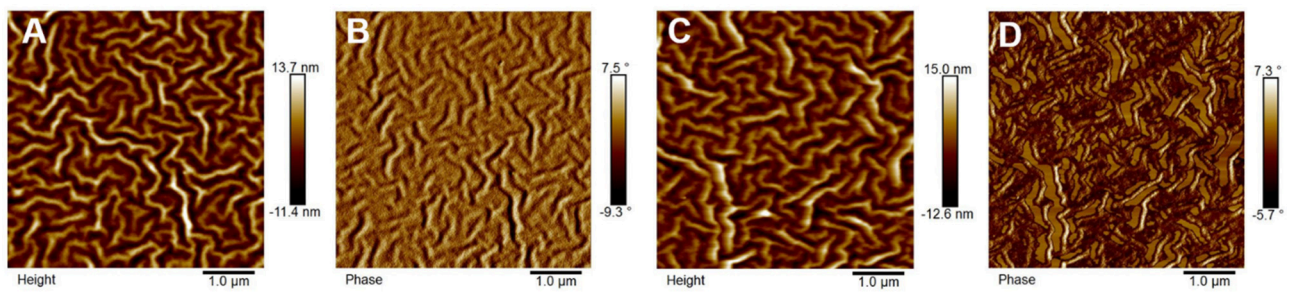

FIGURE 4 | AFM **(A,C)** height and **(B,D)** phase image of PTB7-Th:PZn-TNI; **(A,B)** in the absence of pyridine and **(C,D)** in the presence of pyridine.

PTB7-Th:P_{Zn}-TNI devices with and without additives show the slope of 2.63 and 1.93 kT/q, respectively. This implies that PTB7-Th:P_{Zn}-TNI devices in the absence of additives have the lowest trap-assisted recombination in anopen-circuit condition. The hole and electron transport properties of PTB7-Th:P_{Zn}-TNI devices were measured by a space-charge-limited-current (SCLC) analysis (**Figures 3C,D**) (Mihailetchi et al., 2005). The electron- and hole-only devices were fabricated with a structure of ITO/ZnO/PTB7-Th:P_{Zn}-TNI/ZnO/Al and ITO/PEDOT:PSS/PTB7-Th:P_{Zn}-TNI/MoO_x/Ag, respectively. In the presence of pyridine additive, the hole and electron mobilities of PTB7-Th:P_{Zn}-TNI were 2.4×10^{-4} and 1.3×10^{-6} $cm^2\ V^{-1}\cdot s^{-1}$, respectively, whereas, in the absence of additives, the hole and electron mobilities were increased to 2.9×10^{-4} and 2.5×10^{-6} $cm^2\ V^{-1}\cdot s^{-1}$, respectively. Thus, it is expected that the pyridine additive worsens the nanomorphology of PTB7-Th:P_{Zn}-TNI devices via excessive intermolecular aggregation.

The morphology of the PTB7-Th:P_{Zn}-TNI active layer was investigated by atomic force microscopy (AFM) (**Figure 4**) and two-dimensional grazing incidence X-ray diffraction (2D-GIXD) analyses (**Figure 5**). In AFM images, PTB7-Th:P_{Zn}-TNI blended film possesses bicontinuous crystalline domains in the absence of additives (**Figures 4A,B**), whereas the addition of pyridine additive intensifies the intermolecular ordering of P_{Zn}-TNI domains, leading to severe phase segregation between PTB7-Th and P_{Zn}-TNI (**Figures 4C,D**). The 2D-GIXD results also support the AFM analysis. Additive-free PTB7-Th:P_{Zn}-TNI film showed clear π-π stacking orientation (010) peak at ∼1.6 $Å^{-1}$ along the q_z axis, which indicates the face-on orientation with a d-spacing of ∼3.9 Å (**Figures 5B,C**). However, the pyridine-treated PTB7-Th:P_{Zn}-TNI film showed the increased π-π stacking

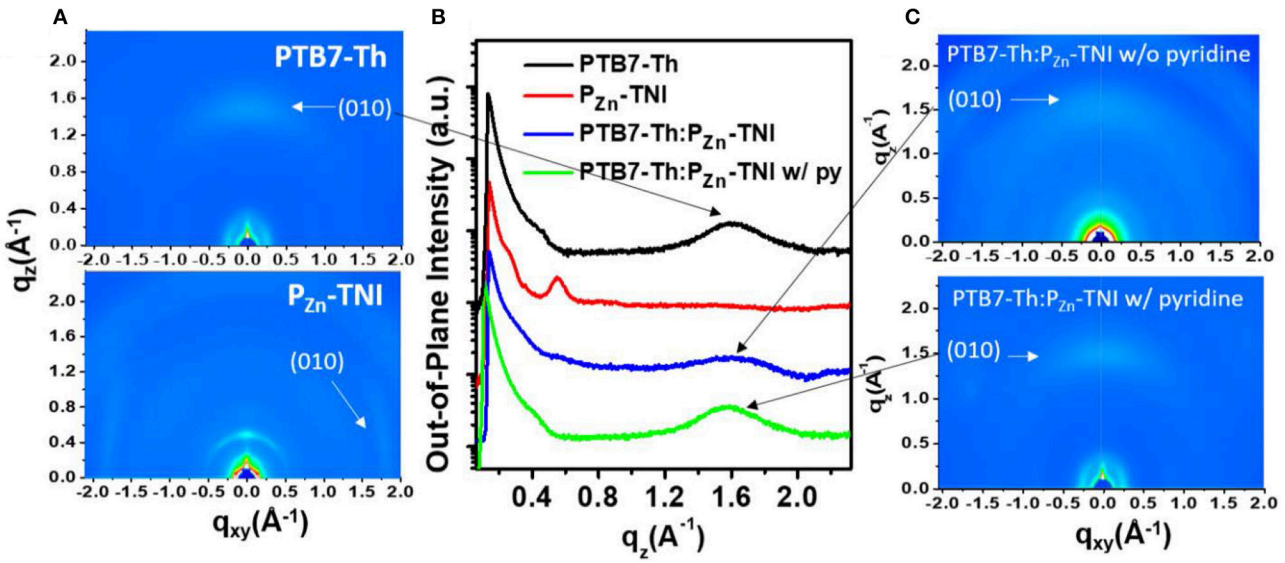

FIGURE 5 | (A) 2D-GIXD images of **(A)** pristine film of PTB7-Th and P_{Zn}-TNI, and **(C)** additive-free PTB7-Th:P_{Zn}-TNI blend film and pyridine-treated one. **(B)** Out-of-plane line-cut of PTB7-Th, P_{Zn}-TNI, and PTB7-Th:P_{Zn}-TNI film.

interaction and induced the phase aggregation (**Figure 5C**). The (010) peak in the blend film is assigned to the orientation of PTB7-Th domains (**Figure 5A**), which implies that the decrease in the photovoltaic performances in presence of pyridine is probably due to the aggregation of the PTB7-Th domains in the PTB7-Th:P_{Zn}-TNI blend film. As a result, the P_{Zn}-TNI having highly planar molecular structure possesses the sizable π-π intermolecular stacking and crystalline nanomorphology in the additive-free solvent system, which means that no more post-treatment is required in PTB7-Th:PZn-TNI blend system. In addition, the additive-free system can prevent undesirable morphological change and photo-oxidation degradation by additives in the active layer (Li et al., 2017).

CONCLUSIONS

We have synthesized a novel porphyrin acceptor, P_{Zn}-TNI, by incorporating four naphthalene imide (NI) units at the meso position of the P_{Zn} core. P_{Zn}-TNI showed unique bimodal absorption with a strong Soret band and a weak Q-band. The insufficient long-wavelength absorption of P_{Zn}-TNI was covered by a low-bandgap donor, PTB7-Th. As a result, bulk heterojunction fullerene-free OSCs composed of P_{Zn}-TNI and PTB7-Th showed panchromatic photon-to-current conversion covering entire area of 300–800 nm. The PTB7-Th:P_{Zn}-TNI devices exhibited a promising PCE of 5.07%, which is the highest and the first promising PCE in the porphyrin-based acceptors except for those utilizing the PDI units. Notably, the additive-free solution process provided the best photovoltaic performance, whereas the pyridine additive had a negative effect on the nanomorphology by the excessive molecular aggregation of the PTB7-Th:P_{Zn}-TNI film. The planar backbone structure of P_{Zn}-TNI assists the sizable molecular ordering in the PTB7-Th:P_{Zn}-TNI film without additive treatment, which is favorable for practical applications.

AUTHOR CONTRIBUTIONS

IJ and SY conceived the ideas and designed the PZn-TNI. U-HL synthesized all the materials and JK assisted the characterization of all the materials. S-YJ supervised all the device fabrication and optimization. WH fabricated all the OSC devices and SE assisted the device characterization.

ACKNOWLEDGMENTS

The authors gratefully acknowledge support from the New and Renewable Energy Core Technology Program of the Korea Institute of Energy Technology Evaluation and Planning (KETEP), granted financial resources from the Ministry of Trade, Industry and Energy, Republic of Korea (No. 20163030013960), the National Research Foundation (NRF) Grant funded by the Korean Government (MSIP, No. 2016R1A5A1012966 and No. 2017R1C1B2010694), and the Global Scholarship Program for Foreign Graduate Students at Kookmin University in Korea.

SUPPLEMENTARY MATERIAL

The Supplementary Material for this article can be found online at: https://www.frontiersin.org/articles/10.3389/fchem.2018.00473/full#supplementary-material

REFERENCES

Azmi, R., Oh, S. H., and Jang, S. Y. (2016). High-efficiency colloidal quantum dot photovoltaic devices using chemically modified heterojunctions. *ACS Energy Lett.* 1, 100–106. doi: 10.1021/acsenergylett.6b00070

Blom, P. W. M., Mihailetchi, V. D., Koster, L. J. A., and Markov, D. E. (2007). Device physics of polymer:fullerene bulk heterojunction solar cells. *Adv. Mater.* 19, 1551–1566. doi: 10.1002/adma.200601093

Che, X., Li, Y., Qu, Y., and Forrest, S. R. (2018). High fabrication yield organic tandem photovoltaics combining vacuum- and solution-processed subcells with 15% efficiency. *Nat. Energy* 3, 422–427. doi: 10.1038/s41560-018-0134-z

Cheng, P., Zhang, M., Lau, T. K., Wu, Y., Jia, B., Wang, J., et al. (2017). Realizing small energy loss of 0.55 eV, high open-circuit voltage >1 V and high efficiency >10% in fullerene-free polymer solar cells via energy driver. *Adv. Mater.* 29:1605216. doi: 10.1002/adma.201605216

Clarke, T. M., and Durrant, J. R. (2010). Charge photogeneration in organic solar cells. *Chem. Rev.* 110, 6736–6767. doi: 10.1021/cr900271s

Duan, Y., Xu, X., Yan, H., Wu, W., Li, Z., and Peng, Q. (2017). Pronounced effects of a triazine core on photovoltaic performance–efficient organic solar cells enabled by a PDI trimer-based small molecular acceptor. *Adv. Mater.* 29:1605115. doi: 10.1002/adma.201605115

Eom, S. H., Kim, H. S., Do, H. J., Lee, U. H., Wibowo, F. T. A., Hwang, D. H., et al. (2018). n-Type core effect on perylene diimide based acceptors for panchromatic fullerene-free organic solar cells. *Dyes Pigments* 156, 318–325. doi: 10.1039/C7PY00497D

Gao, K., Li, L., Lai, T., Xiao, L., Huang, Y., Huang, F., et al. (2015). Deep Absorbing porphyrin small molecule for high-performance organic solar cells with very low energy losses. *J. Am. Chem. Soc.* 137, 7282–7285. doi: 10.1021/jacs.5b03740

Hadmojo, W. T., Nam, S. Y., Shin, T. J., Yoon, S. C., Jang, S. Y., and Jung, I. H. (2016). Geometrically controlled organic small molecule acceptors for efficient fullerene-free organic photovoltaic devices. *J. Mater. Chem. A* 4, 12308–12318. doi: 10.1039/C6TA04344E

Hadmojo, W. T., Yim, D., Aqoma, H., Ryu, D. Y., Shin, T. J., Kim, H. W., et al. (2017). Artificial light-harvesting n-type porphyrin for panchromatic organic photovoltaic devices. *Chem. Sci.* 8, 5095–5100. doi: 10.1039/C7SC01275F

Hadmojo, W. T., Yim, D., Sinaga, S., Lee, W., Ryu, D. Y., Jang, W. D., et al. (2018). Near-infrared harvesting fullerene-free all-small-molecule organic solar cells based on porphyrin donors. *ACS Sustain. Chem. Eng.* 6, 5306–5313. doi: 10.1021/acssuschemeng.8b00010

Hou, J., Inganäs, O., Friend, R. H., and Gao, F. (2018). Organic solar cells based on non-fullerene acceptors. *Nat. Mater.* 17:119. doi: 10.1038/nmat5063

Kim, Y., Cook, S., Tuladhar, S. M., Choulis, S. A., Nelson, J., Durrant, J. R., et al. (2006). A strong regioregularity effect in self-organizing conjugated polymer films and high-efficiency polythiophene:fullerene solar cells. *Nat. Mater.* 5:197. doi: 10.1038/nmat1574

Li, G., Zhu, R., and Yang, Y. (2012). Polymer solar cells. *Nat. Photonics* 6:153. doi: 10.1038/nphoton.2012.11

Li, H., He, D., Mao, P., Wei, Y., Ding, L., and Wang, J. (2017). Additive-free organic solar cells with power conversion efficiency over 10%. *Adv. Energy Mater.* 7:1602663. doi: 10.1002/aenm.201602663

Li, N., Ke, G., Feng, L., Yuanyuan, K., Xiaofang, J., Linlin, L., et al. (2016). 11% efficient ternary organic solar cells with high composition tolerance via integrated near-IR sensitization and interface engineering. *Adv. Mater.* 28, 8184–8190. doi: 10.1002/adma.201602834

Liang, N., Jiang, W., Hou, J., and Wang, Z. (2017). New developments in non-fullerene small molecule acceptors for polymer solar cells. *Mater. Chem. Front.* 1, 1291–1303. doi: 10.1039/C6QM00247A

Liang, Y., Xu, Z., Xia, J., Tsai, S. T., Wu, Y., Li, G., et al. (2010). For the bright future—bulk heterojunction polymer solar cells with power conversion efficiency of 7.4%. *Adv. Mater.* 22, E135–E138. doi: 10.1002/adma.200903528

Liao, S. H., Jhuo, H. J., Cheng, Y. S., and Chen, S. A. (2013). Fullerene derivative-doped zinc oxide nanofilm as the cathode of inverted polymer solar cells with low-bandgap polymer (PTB7-Th) for high performance. *Adv. Mater.* 25, 4766–4771. doi: 10.1002/adma.201301476

Lin, Y., Zhao, F., Wu, Y., Chen, K., Xia, Y., Li, G., et al. (2017). Mapping polymer donors toward high-efficiency fullerene free organic solar cells. *Adv. Mater.* 29:1604155. doi: 10.1002/adma.201604155

Mandoc, M. M., Veurman, W., Koster, L. J. A., de Boer, B., and Blom, P. W. M., et al. (2007). Origin of the reduced fill factor and photocurrent in MDMO-PPV:PCNEPV all-polymer solar cells. *Adv. Funct. Mater.* 17, 2167–2173. doi: 10.1002/adfm.200601110

Marcus, R. A. (1963). On the theory of oxidation—reduction reactions involving electron transfer. v. comparison and properties of electrochemical and chemical rate constants. *J. Phys. Chem.* 67, 853–857. doi: 10.1021/j100798a033

Mihailetchi, V. D., Wildeman, J., and Blom, P. W. M. (2005). Space-charge limited photocurrent. *Phys. Rev. Lett.* 94:126602. doi: 10.1103/PhysRevLett.94.126602

Mihailetchi, V. D., Xie, H. X., de Boer, B., Koster, L. J. A., and Blom, P. W. M. (2006). Charge transport and photocurrent generation in poly(3-hexylthiophene): methanofullerene bulk-heterojunction solar cells. *Adv. Funct. Mater.* 16, 699–708. doi: 10.1002/adfm.200500420

Tang, A., Chen, F., Chen, B., Tan, Z. A., Yang, J., Li, J., et al. (2018). Utilizing benzotriazole and indacenodithiophene units to construct both polymeric donor and small molecular acceptors to realize organic solar cells with high open-circuit voltages beyond 1.2 V. *Front. Chem.* 6:147. doi: 10.3389/fchem.2018.00147

Wu, Q., Zhao, D., Schneider, A. M., Chen, W., and Yu, L. (2016). Covalently bound clusters of alpha-substituted pdi-rival electron acceptors to fullerene for organic solar cells. *J. Am. Chem. Soc.* 138, 7248–7251. doi: 10.1021/jacs.6b03562

Yan, C., Barlow, S., Wang, Z., Yan, H., Jen, A. K. Y., Marder, S. R., et al. (2018). Non-fullerene acceptors for organic solar cells. *Nat. Rev. Mater.* 3:18003. doi: 10.1038/natrevmats.2018.3

Yao, H., Ye, L., Hou, J., Jang, B., Han, G., Cui, Y., et al. (2017). Achieving highly efficient nonfullerene organic solar cells with improved intermolecular interaction and open-circuit voltage. *Adv. Mater.* 29:1700254. doi: 10.1002/adma.201700254

Yen, W. N., Lo, S. S., Kuo, M. C., Mai, C. L., Lee, G. H., Peng, S. M., et al. (2006). Synthesis, structure, and optical and electrochemical properties of star-shaped porphyrin–triarylamine conjugates. *Org. Lett.* 8, 4239–4242. doi: 10.1021/ol061478w

Zhan, C., Zhang, X., and Yao, J. (2015). New advances in non-fullerene acceptor based organic solar cells. *RSC Adv.* 5, 93002–93026. doi: 10.1039/C5RA17715D

Zhang, A., Li, C., Yang, F., Zhang, J., Wang, Z., Wei, Z., et al. (2017). An electron acceptor with porphyrin and perylene bisimides for efficient non-fullerene solar cells. *Angew. Chem. Int. Ed.* 56, 2694–2698. doi: 10.1002/anie.201612090

Zhang, Y., Wan, Q., Guo, X., Li, W., Guo, B., Zhang, M., et al. (2015). Synthesis and photovoltaic properties of an n-type two-dimension-conjugated polymer based on perylene diimide and benzodithiophene with thiophene conjugated side chains. *J. Mater. Chem. A* 3, 18442–18449. doi: 10.1039/C5TA05014F

Zhao, F., Dai, S., Wu, Y., Zhang, Q., Wang, J., Jiang, L., et al. (2017). Single-junction binary-blend nonfullerene polymer solar cells with 12.1% efficiency. *Adv. Mater.* 29:1700144. doi: 10.1002/adma.201700144

Zhao, J., Li, Y., Yang, G., Jiang, K., Lin, H., Ade, H., et al. (2016). Efficient organic solar cells processed from hydrocarbon solvents. *Nat. Energy* 1:15027. doi: 10.1038/nenergy.2015.27

Zhao, W., Li, S., Yao, H., Zhang, S., Zhang, Y., Yang, B., et al. (2017). Molecular optimization enables over 13% efficiency in organic solar cells. *J. Am. Chem. Soc.* 139, 7148–7151. doi: 10.1021/jacs.7b02677

Zhao, W., Qian, D., Zhang, S., Li, S., Inganäs, O., Gao, F., et al. (2016). Fullerene-free polymer solar cells with over 11% efficiency and excellent thermal stability. *Adv. Mater.* 28, 4734–4739. doi: 10.1002/adma.201600281

Conflict of Interest Statement: The authors declare that the research was conducted in the absence of any commercial or financial relationships that could be construed as a potential conflict of interest.